Contrib Mineral Petrol (1984) 88:217–232

Contributions to Mineralogy and Petrology

Carbon dioxide in petrogenesis III: role of volatiles in the ascent of alkaline magma with special reference to xenolith-bearing mafic lavas

Frank J. Spera
Department of Geology and Geophysical Sciences, Princeton University, Princeton, NJ 08544, USA

Abstract. Kinetic and fluid dynamic constraints on deep-seated magma migration rates suggest ascent velocities in the range 10 to 30 m/s, 10^{-1} to 10 m/s and 10^{-2} to 5 m/s for kimberlitic, garnet peridotite-bearing and spinel peridotite-bearing alkalic magmas. These rates virtually demand translithospheric magma transport by a fracture as opposed to diapiric mechanism. The hypothesis that volatile exsolution accelerates magma through the deep lithosphere is tested by solution of the appropriate set of conservation, mass balance and volatile component solubility equations governing the steady ascent (decompression) of compressible, two-phase magma (melt + H_2O + CO_2) in which irreversible phenomena (friction, heat transfer) are accounted for. The results of the numerical experiments were designed to test the importance of melt bulk composition (kimberlite, nephelinite, alkali basalt), initial conditions (mass flux ($\dot{M}$), heat transfer coefficient (B), lumped friction factor (C_f)), conduit width (D), initial magma volatile content and geothermal gradients. The fractional increase in ascent rate ($\Delta u/u_i$) is rarely greater than approximately 2 during translithospheric migration. The propellant hypothesis is rejected as a first-order mechanism driving magma acceleration during ascent. The most influential parameters governing ascent dynamics are $\dot{M}$, C_f, D, B and the geotherm. Because of the relatively incompressible nature of the magmatic volatile phase at $P > 100$ MPa, the initial magma volatile content plays a secondary (although demonstrable) role. The main role of volatiles is in controlling the initial magma flux ($\dot{M}$) and the magma pressure during ascent. In adiabatic ($B = 0$) simulations, magma ascends nearly isothermally. Generally, however, the assumption of adiabaticity is a poor one especially for flow through narrow (0.5 to 2 m) conduits in old (cold) lithosphere at rates $\sim 10^{-1}$ m/s. The proposed fluid dynamic model is consistent with and complementary to the magma-driven crack propagation models. The generation of mantle metasomatic fluid is a corollary of the non-adiabatic ascent of volatile-bearing magma through the lithosphere. Magma heat death is an important process for the creation of mantle heterogeneity.

Introduction

Preamble

This paper is the third in a four part series dealing with the role of volatiles in petrogenesis, focusing particularly on mantle metasomatism and the eruption and transport history of mafic alkalic magma. In part I (Spera and Bergman 1980), it was noted that CO_2 solubility data for natural and synthetic silicate liquids at high temperatures and pressures are consistent with a solution mechanism represented schematically by a polymer condensation reaction of the form:

$$SiO_4^{-4}\,(\text{melt}) + CO_2(\text{v}) + Si_n\,O_{3n+1}^{-2(n+1)}\,(\text{melt}) \rightleftharpoons Si_{n+1}\,O_{3n+4}^{-2(n+2)}\,(\text{melt}) + CO_3^{-2}\,(\text{melt})$$

where n is a positive integer. Thermodynamic analysis of available $X^m_{CO_2} - P_t - T$ data enabled determination of the equilibrium CO_2 content of alkalic, tholeiitic and andesitic melts as a function of CO_2 fugacity, total pressure and temperature. Unlike H_2O, the CO_2 content of saturated melt depends markedly on the bulk composition of that melt. CO_2 is most soluble in low silica – high alkali activity melts. Indeed, as noted by Wyllie and Huang (1976), Wyllie (1978, 1979) and by Eggler (1974, 1978), the genesis of very low a_{SiO_2} melt may depend critically upon a non-trivial content of total carbon in the mantle source. According to Wyllie (1980) for instance, at depths greater than about 80 km, partial fusion of anhydrous carbonated mantle peridotite produces a trace of carbonatitic magma (30 to 40 wt.% CO_2) which changes with increasing temperature (hence degree of partial melting) through compositions corresponding to kimberlite and olivine-melilite nephelinite. Precise melt compositions depend on the bulk composition of the source, P_t, T, f_{CO_2}, f_{H_2O}, and f_{O_2}.

Additional information bearing on the significance of volatile components in alkalic magmatism was summarized in part II of this series (Spera 1981). Specifically, abundant petrographic, fluid inclusion, geochemical and isotopic evidence from xenoliths in alkali basalts suggests that low-viscosity fluids rich in O–H–C–S–Cl–F, dissolved silicates and especially the incompatible elements may ascend, decompress and precipitate crystalline phases and/or induce partial fusion in the upper mantle (e.g., see Boettcher et al. 1979; Boettcher and O'Neil 1980; Bailey 1982). In order to model the dynamics and thermodynamics of ascending mantle metasomatic fluid, the ordinary differential equations expressing conservation of mass, momentum and energy taking account of irreversible effects such as fluid friction and heat transfer (i.e., non-isentropic, non-adiabatic flow) were solved for a variety of initial conditions. The numerical simulations carried out were applicable to the ascent (decompression) of a compressible, viscous, two-component (H_2O–CO_2) non-ideal fluid through a rough vertical crack of constant width. For a given set of initial conditions, the variation of fluid density, velocity, tempera-

Offprint requests to: F.J. Spera

ture and pressure with distance along the crack depends on a number of transport (e.g., fluid thermal conductivity, viscosity, etc.), thermodynamic (e.g., composition, equation of state, the isobaric heat capacity, etc.) and geometric (e.g., crack width, tortuosity, etc.) parameters, some of which are poorly constrained. However, based on a range of geologically reasonable parameters, the following conclusions were reached: 1) Metasomatic fluid moves at uniform rates of order 1 m/s following a short transient phase of acceleration, 2) the fluid expands and ascends along a nearly isothermal path and 3) the fluid acts as an efficient heat transfer agent capable of locally raising temperatures perhaps even to that of the local peridotite solidus. An additional implication of the rapid movement and decompression of mantle metasomatic fluid (MMF) is the generation of local isotopic and trace element heterogeneity along the ascent path.

A continuum of flow regimes are possible for magmatic flows. At one extreme is the adiabatic ascent of incompressible melt-dominated magma. At the other end of the spectrum, there is the movement of metasomatic fluid. In this paper and in part IV of this series, attention is focused on magmatic flows of an intermediate nature. Such flows are intrinsically multiphase (crystals + melt + vapor) with a thermodynamic path that is neither isentropic nor adiabatic. Specifically, the thermodynamics and fluid mechanical evolution of volatile-charged magma during ascent through the lithosphere is addressed. The petrological and geochemical implications of thermal crises in terms of the creation of mantle heterogeneity, the generation of metasomatic fluid and the focusing and upward transport of mantle heat are not discussed except in a general way. Instead attention is focused on magma transport phenomena of direct relevance to the ascent and eruption of alkali basaltic magma. The outline for the remainder of this paper is given below.

Following a brief synopsis of the thermal crisis concept, a discussion of the evidence bearing on deep-seated ascent rates is presented. It has been suggested that a high concentration of volatiles in mafic alkalic magma provides a source for the rapid generation of magma kinetic energy by PV work associated with decompression, volatile degassing and vapor phase expansion. In order to test this hypothesis, a fluid dynamic model of multiphase conduit flow is developed. This model is similar to one developed earlier (part II) in that irreversible effects (i.e., sources of entropy-production) are explicitly considered. However, the model proposed here goes beyond the earlier one in that the analysis models the *two-phase* (melt plus vapor) nature of volatile-saturated magma. Melt solubility expressions for H_2O and CO_2 are combined with the equations of change (conservation equations) so that the amount and composition of the vapor phase may be determined as a function of height above the magma source reservoir. Additionally, the H_2O and CO_2 content of the melt, assumed to be in equilibrium with the vapor phase, may also be determined as a function of height. In the final section, the results of a number of numerical simulations are presented and discussed in relation to traditional kinds of geologic evidence.

Magma heat death: a secondary origin for MMF

A well-defined mechanism for the generation of MMF that is consistent with theoretical deductions from heat-transfer theory, the probable sizes of magma transport conduits and the petrology of mantle xenoliths involves the liberation of volatiles as a consequence of crystallization of volatile-bearing magma due to non-adiabatic ascent. In this view, magma with some initial volatile content undergoes significant heat loss (see below) upon ascent. Crystallization occurs within the conduit as magma moves upwards. This process has been termed flow crystallization by Irving (1980). Depending on the prevailing local values of temperature, pressure, and other intensive thermodynamic variables, hydrous, carbonate or sulphide phases may or may not precipitate as crystallization proceeds. In cases where the crystallizing assemblage does not accommodate the initial complement of volatiles, a fluid phase containing dissolved silicate components (Ryabchikov and Boettcher 1980; Ryabchikov et al. 1982) is generated. Because of differences in the PT stability of possible volatile-bearing phases and melt/vapor partitioning of volatile components, the composition of MMF may be quite different from the initial volatile composition of the alkaline magma. Solubility relations indicate that the vapor phase is enriched in CO_2 relative to H_2O, the latter being concentrated in coexisting melt and/or hydrous-bearing phases at high pressure. The common occurrence of CO_2-rich fluid inclusions in many types of mantle xenoliths (Roedder 1965; Murck 1978; Bergman 1982; Solovova et al. 1984; Lovelace 1984) may be a reflection of this partitioning effect. A typical abundance of CO_2-rich fluid inclusions in olivine-bearing ultramafic rocks is 0.1 vol % (Bergman et al. 1981). If a fluid density of 800 kg/m^3 is considered average (Murck et al. 1978), then one calculates a bulk C content of about 70 wt. ppm. This is within the range of measured concentrations of 60 to 180 wt. ppm for olivine single crystals from San Carlos, Arizona Type I nodules (Oberheuser et al. 1983).

Other hypotheses have been proposed to explain the abundance of CO_2-rich inclusions within olivine-rich peridotites (Freund et al. 1980, 1983). A major uncertainty is the amount of C that may be dissolved in olivine and pyroxene under mantle conditions.

The thermal crisis argument hinges critically on the non-adiabatic ascent of magma. Many petrologists assume magma ascent within the lithosphere to be an adiabatic process despite strong theoretical evidence for the contrary (e.g., see Marsh 1976, 1978; Marsh and Kantha 1978; Spera 1977, 1982; Delaney and Pollard 1982). Even in diapiric models where the surface area to volume ratio of the ascending magma body is relatively small, heat losses can be significant due to turbulent convection (Carmichael et al. 1977; Morris 1982). The main parameters governing heat loss during magma ascent include the ascent rate, the size and shape of the magma body and the local thermal gradient in the lithosphere through which magma rises.

Evidence is now mounting to suggest that, within the lithosphere, basaltic magma is transported upwards by viscous flow through a crack network (i.e., swarms of propagating melt-filled fractures). This concept has been discussed recently by Shaw (1980), Stevenson (1983), and Spence and Turcotte (1983) and is supported by field studies of frozen magma conduits (e.g., dike swarms along axes of exhumed shield volcanoes and rift zones (Walker 1958, Swanson et al. 1975), seismic studies of volcanic tremor and earthquake swarms related to magma migration (Aki et al. 1977; Aki and Koyanagi 1981; Hill 1977) and ground de-

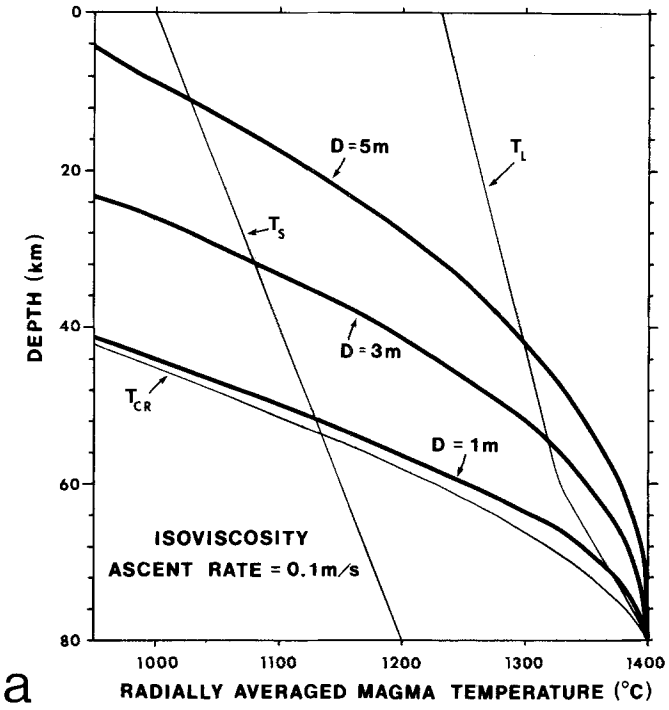

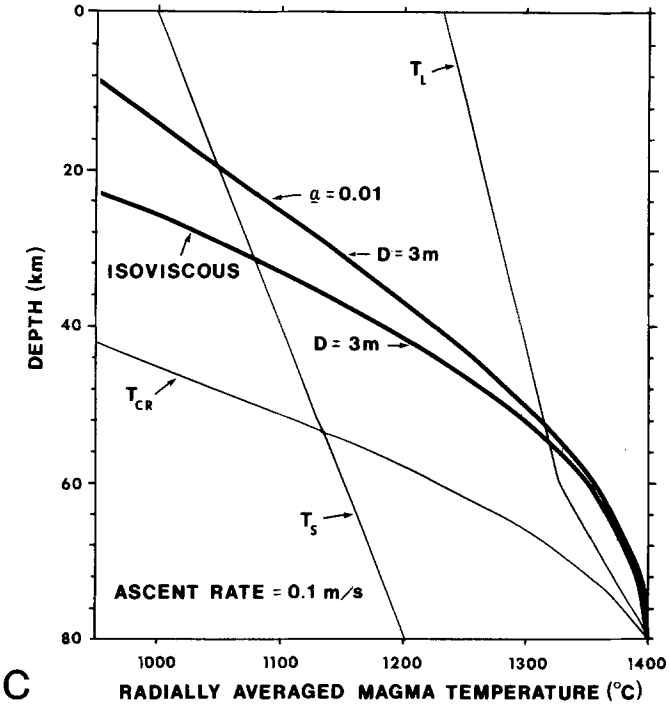

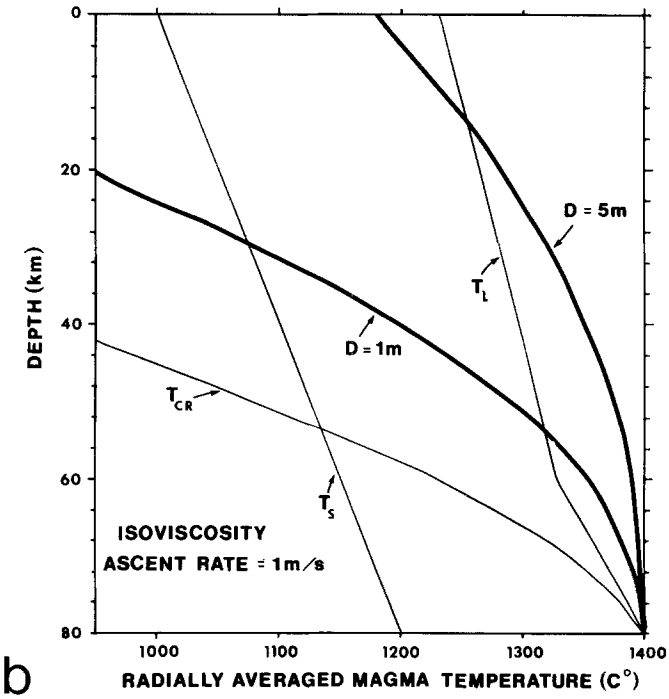

Fig. 1a–c. Calculated temperature-depth trajectories for non-adiabatic ascent of magma at constant velocity in a cylindrical pipe. Details of the simplified model are set out in Appendix I. The light curves labeled T_{CR}, T_S and T_L represent the geotherm and the solidus and liquidus curves for a basanite (Arculus 1975). The geotherm was taken such that $T=1{,}400°$ C at 80 km and $T=0°$ C at the surface. This implies a near surface geothermal gradient of 26° C/km. Clinopyroxene is the liquidus phase for depths greater than about 60 km; at shallower depths olivine is on the liquidus. The transformation from pressure to depth is made by assuming a "normal" continental crustal structure: 30 km of sialic crust of density 2,650 km/m^3 and a submoho density of 3,300 kg/m^3. **a** Constant viscosity case for average ascent rate of 10 cm/s. Temperature trajectories are plotted for initial cylindrical duct diameters of 1, 3 and 5 m. **b** Isoviscous case for ascent velocity of 1 m/s and tube diameters of 1 and 3 m. **c** $u=10^{-1}$ m/s, $D=3$ m and the coefficient a, a measure of the temperature dependence of magma viscosity is equal to 0 (isoviscous) or 0.01. The heat transfer model breaks down for larger values of a. Note that temperatures calculated here are *maximum* estimates since (1) a cylindrical conduit has been assumed and (2) magma compressibility effects have been ignored. Heat transfer is much greater for magma transport through a planar crack. The isentropic gradient for magma is approximately $-1°$ C/km. If these two factors were taken into account, heat death for magma rise in conduits several meters in width would be even more prevalent

formation studies at active volcanos (Ryan et al. 1983; Hauksson 1983). Apparently, the characteristic width of magma-filled basaltic conduits is measured in meters. Conduit lengths are more difficult to estimate. A maximum value is the depth to the source reservoir, perhaps many tens of kilometers for single long cracks. It is concluded that basaltic conduits are characterized by relatively large surface area to volume ratios. On this ground alone, heat transfer between magma and surrounding lithosphere may be expected to be important.

In terms of magma ascent rates, indirect evidence based on the competence of nearly aphyric magma to transport dense xenoliths (see below), rates of migration of earthquake swarms related to magma transport (Klein et al. 1977; Klein 1982; Hauksson 1983) and calculations for magma ascent in dike or pipe-like conduits (Spera 1980), suggest characteristic ascent rates in the range cm/s to m/s for alkali basaltic magma (see below).

On the basis of the above inferences and a simple heat transfer model (Appendix 1) it is suggested that much of the magma generated in the mantle never reaches the surface of the Earth (Fig. 1). This conclusion is consistent with those of Crisp (1983) regarding the volume ratio of intrusives to extrusives at any given volcano-plutonic center. Her approach was based on an examination of the systematics of long-term ($10^2 < t < 10^8$ yrs) volumetric rates of in-

trusion and extrusion of magma as a function of crustal thickness and composition, magma composition and tectonic environment. Restricting attention to about ten well-documented magmatic systems where the volcano-plutonic link is especially good, she noted extrusive to intrusive volume ratios between about 1:4 to 1:20, the former being applicable to basaltic systems in oceanic (thin crust) environments.

In summary then, it is suggested that MMF may originate by freezing of volatile-bearing, and ultimately volatile saturated magma at depth. Evolution of a free vapor phase is an obvious corollary of magma crystallization as is the generation of trace element, and with time, isotopic heterogeneity within restricted portions of the lithosphere. A prediction of the thermal crisis hypothesis is that magma stagnation at depth should be most common in regions characterized by cold, thick lithosphere. In fact, some of the most convincing evidence for mantle metasomatism (modal metasomatism) comes from xenoliths derived from the subcontinental lithosphere (Harte 1983).

Magma ascent rates

Introduction

Data bearing on the ascent rate of magma within the deep lithosphere are difficult to acquire. However, because the rate of magma transport is an important parameter in constraining petrogenetic theories, an attempt is made to summarize available evidence. Although no single inference or calculation is free from ambiguity, when considered collectively, there are indications that magma ascent rates on the order of cm/s to m/s are not uncommon. These characteristic velocities refer to averages over the ascent path in situations where magma successfully traverses the lithosphere. It must be kept in mind that such instances are probably in the minority; much of the magma generated in the deep lithosphere or asthenosphere may never reach the surface.

Kimberlites

Although the present contribution focuses primarily on the dynamics and energetics of alkali basalt ascent and eruption, it is important to note that in nature a continuous spectrum of flow regimes across the compositional range carbonatite-kimberlite-alkaline basalt exists. Rheological and volatile-content variations across this compositional spectrum are associated with contrasting dynamic flow regimes. For example, kimberlites which consist of roughly subequal portions of solid (xenocrysts, phenocrysts, lithic inclusions), melt and vapor almost certainly ascend more rapidly than melt-dominated alkalic basaltic magma. Kimberlite ascent rates can be estimated by a number of methods including 1) reconciliation of the sizes of annealed olivine crystals with experimental coarsening kinetics data (Mercier 1979) 2) the size and spacing of exsolved pigeonite domains parallel to (001) in host diopsidic pyroxene (McCallister et al. 1979; Grove 1982), 3) rates of graphitization of diamond at high temperatures and pressure (Horton and Horton 1972), 4) preservation of coesite in grospydite inclusions such as those from the Roberts Victor kimberlite pipe, South Africa (Smyth and Hatton 1977) and 5) theoretical models of kimberlite eruptions (McGetchin and Ullrich 1973; McGetchin and Nikhanj 1973; Anderson 1979). Ascent rates calculated by this author based on the above considerations generally lie in the range 10 to 30 m/s, and are higher by about an order of magnitude than estimates for alkali basaltic magma as noted below.

Alkali basalt ascent rates: kinetic constraints

Based on rate information garnered from phase equilibrium studies (Cohen et al. 1967; Millhollen et al. 1974; Millhollen and Wyllie 1974; O'Hara et al. 1971) crude estimates of xenolith residence times can be made for garnet bearing lherzolites. For example, Chapman (1976) has described garnet-bearing type I peridotite nodules from basanitic tuffs in Scotland. The preservation of garnet-bearing inclusions within these tuffs and lavas suggests xenolith residence times around four to eight hours and minimum capture depths of about 75 km at 1,200° C. This implies ascent rates near 2 to 5 m/s for these particular basanites.

Many workers have noted petrographic or geochemical evidence for intranodule partial melting, especially in type I xenoliths (e.g., Vilminot 1965; White 1966; Cooper and Green 1969; Kleeman et al. 1969; Littlejohn and Greenwood 1974; Frey and Green 1974; Frey and Prinz 1978; Ghent et al. 1980; Fujii and Scarfe 1982). Although an original patchy distribution of hydrous phases such as pargasitic amphibole or phlogopite has been called upon to explain the presence and localization of partial melt in some instances (e.g., see Frey and Green 1974), partial melting has been noted in nodules that presently contain no hydrous phases (e.g., Fujii and Scarfe 1982; Ghent et al. 1980). The extent of partial melting is usually quite small (<1 vol %). Melt may originate by partial *in situ* fusion during rapid heating and decompression due to xenolith incorporation into hotter magma. In the absence of detailed melting rate studies it is impossible to precisely determine xenolith residence times. However, the preservation of chemical heterogeneity in melt patches within spinel lherzolites may be used to obtain maximum xenolith residence times and hence constrain ascent rates. Frey and Green (1974) report, for instance, heterogeneity with respect to CaO in small melt patches in lherzolites from Victorian basanites. The diffusion time for eradication of CaO heterogeneity in a melt inclusion of, say, 2 mm width (see plate 10 in Littlejohn and Greenwood 1974) is about 3 days based on the Ca diffusion data of Hofmann and Magaritz (1977) at 1,200° C. Since heterogeneity of CaO is preserved, the nodule residence time must have been *less* than 3 days (approximately). The *minimum* ascent rate averaged over the distance traversed by the nodule (assumed to be 60 km) is therefore 20 cm/s.

On the basis of a lack of chemical zoning in spinel and clinopyroxene grains adjacent to melt in patches in spinel lherzolites from British Columbia, Fujii and Scarfe (1982), determined a minimum basalt ascent rate of 2 m s^{-1}. They noted that this rate is in agreement with calculations based on Stokes' law assuming newtonian behavior of the magma.

A second independent line of evidence for ascent rates comes from experiments on annealing rates of fractures in olivine at high temperatures (Wanamaker et al. 1982). Although again it is impossible to be precise, experimentally measured annealing rates suggest that healing of 0.2 to 0.5 mm long cracks in Fo_{90} crystals taken from a harzburgite nodule occurs in 3 days to 1 week at 1,200° C near

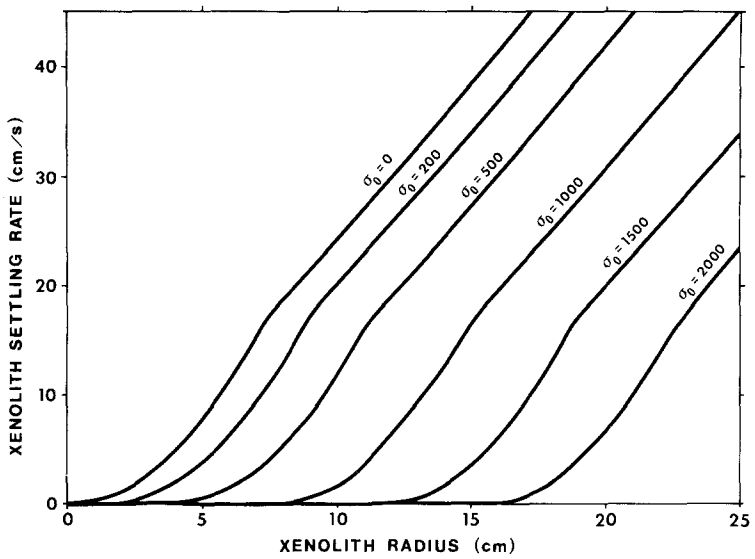

Fig. 2. Illustrative plot of xenolith settling rate versus xenolith radius as a function of magma yield strength (σ_0). Xenoliths are assumed to be spherical. The density difference between xenolith and melt is taken as 500 kg/m^3, the melt density is 2,800 kg/m^3 and a Bingham rheology is assumed with a plastic viscosity of 35 kg m^{-1} s^{-1} (350 poise). Units of yield strength are in N/m^2. A yield strength of 10^2 N/m^2 corresponds roughly to a crystallinity (volume percent) of about 25%. The change in slope on the constant yield strength curves is due to the increasing importance of inertia relative to friction and buoyancy forces at high xenolith Reynolds numbers

QFM oxygen buffer conditions. Since planar features, often crowded with CO_2-rich fluid inclusions, are not unusual in olivine crystals within type I nodules, it is reasonable to assume residence times on the order of 80 to 170 h. If xenolith entrapment occurs at a nominal depth of 60 km (in the spinel lherzolite field) mean ascent rates around 10 to 20 cm/s are indicated. Although the use of crack healing rates as an ascent speedometer for alkalic magma is, at present, only semi-quantitative, it is hoped that further study of the effects of f_{O_2}, P, volatile composition and mineralogy on crack healing rates will better constrain ascent rate determinations (Wanamaker 1984, pers. comm.).

In summary, it is noted that ascent rates in the range 10 cm/s to a few m/s appear to be representative of alkali basaltic magma. Garnet-bearing inclusions are much less commonly found in alkali basalts. When present, they indicate ascent speeds in the range 1 to 10 m/s, approximately. Based on a different set of speedometers (e.g. olivine subgrain coarsening kinetics, diamond graphitization rates, xenolith settling rates, etc.), it is estimated that kimberlites ascend at significantly higher rates, in the range 10 to perhaps 30 m/s.

Alkali basalt ascent rates: inferences from xenolith sizes

Alkali basaltic lava flows and associated tephra deposits commonly contain dense mantle-derived xenoliths. Mantle xenoliths are important not only for the wealth of geochemical information they provide but also because they represent a unique opportunity to investigate deep-seated rates of magma transport. By balancing inertial, viscous and buoyancy forces and taking account of possible non-newtonian behavior of phenocryst or megacryst-laden magma, an average xenolith settling rate may be determined. Obviously the settling rate so computed is a *minimum* estimate of the magma ascent rate.

In Fig. 2, the results of representative xenolith settling calculations are presented. The relations depicted in the figure are based on rheologic data from a number of sources (Shaw 1965, 1969, 1972, 1980; Shaw et al. 1968; Sparks et al. 1977; Pinkerton and Sparks 1978; Murase and McBirney 1973; Feigenson and Spera 1981; Feigenson 1981; Spera, unpubl. data) and expressions derived in Spera (1980). For spherical xenoliths and assuming Bingham plastic rheological behavior (i.e., $\sigma=\sigma_0+\eta\dot{\varepsilon}$, where σ, σ_0, η and $\dot{\varepsilon}$ represent the shear stress, yield strength, viscosity coefficient and strain rate respectively) the following expressions for the nodule settling speed (U_n) were found: For $\mathrm{Re}_n > 2.0$,

$$U_n = 0.344 \left(\frac{\Delta\rho g}{\rho_l}\right)^{5/7} \left(\frac{\rho_l}{\eta_l}\right)^{3/7} \left(R_n - \frac{15\sigma_0}{4\Delta\rho g}\right)^{8/7} \quad (1)$$

whereas for $\mathrm{Re}_n < 2.0$,

$$U_n = \frac{2}{9}\frac{\Delta\rho g}{\eta_l}\left(R_n - \frac{15\sigma_0}{4\Delta\rho g}\right)^2. \quad (2)$$

The nodule Reynolds number (Re_n) is defined as $\rho_l D_n U_n/\eta_l$.

Table 1. Parameters in Eq. (1) and (2)

U_n	nodule settling rate
$\Delta\rho$	$\rho_n - \rho_l$
ρ_n	nodule density
ρ_l	melt density
η_l	plastic viscosity for Bingham magma
g	acceleration due to gravity
R_n	nodule radius (assumed spherical)
Re_n	nodule Reynolds number, $\equiv \rho_l D_n U_n/\eta_l$
D_n	nodule diameter, $\equiv 2R_n$
σ_0	magma yield strength

Parameters appearing in eqs (1) and (2) are defined in Table 1. Equation (1) corrects a typographic error in Eq. (29) in Spera (1980). As an example, calculations suggest a minimum magma ascent rate of about 10 cm/s for transport of a 20 cm diameter spherical nodule in a magma consisting of about 15 vol % phenocrysts. In such a magma the yield strength is approximately 50 N m^{-2}.

The yield strength of magma rapidly rises as the crystallinity increases. Marsh (1981) has ascribed the general rarity of eruptive rocks containing more than 50 vol % phenocrysts to the abrupt change in apparent viscosity at this crystallinity. For Bingham plastic or viscoplastic materials, the apparent viscosity correlates well with the yield strength (σ_0). Indeed, Sparks et al. (1977) have argued that the common occurence of xenoliths in alkalic basalts is due not

to their more rapid ascent rates compared to other basaltic types but, instead, due to their higher yield strengths and, hence, ability to suspend solids. While this author agrees that crystals will, in general, impart a yield strength to magma (it is common knowledge that most multiphase media exhibit yield strength behavior), he does not concur with the conclusion that the high abundance of nodules in the mafic alkaline suite is a consequence of their intrinsically high crystal content (hence yield strength). If this argument was correct, one would expect xenolith-bearing lavas to be laden with a significant (>25%) fraction of *high pressure* phenocrysts since peridotitic xenoliths must be captured at sub-moho depths. Although megacrysts are common in some alkali basalts, their concentration is usually quite low (several volume percent). In addition, in a number of Quaternary Alkali basalts fields in the Western USA this author is personally familiar with (e.g., Lunar Crater Volcanic Field (Bergman 1982), Hawi Series, Kohala Mountain, Hawaii (Feigenson 1981); Grand Canyon National Monument Area, Arizona (Best 1970, 1974a, 1974b), Cima Dome Volcanic Field, Baker, California, San Francisco Peaks Volcanic Area, near Flagstaff, Arizona), no general correlation between phenocryst, megacryst and xenolith content is apparent. Adjacent cones or lava flows from even a single field exhibit large variations in xenolith type, size and abundance with no apparent relationship to lava or tephra crystal content and hence yield strength. Based on the yield strength argument, one might predict that xenoliths would be most abundant in highly phyric basalts and especially basaltic andesites and andesites from stratovolcanoes in island arc settings. This, however, is not the case. On the basis of rheologic data (references previously cited) and the theoretical studies of eruption probability by Marsh (1981), it is suggested that when a magma has cooled sufficiently to produce a high yield strength, its apparent viscosity is so enormous that the magma ascent rate becomes vanishingly small.

Until conclusive evidence for characteristically large yield strengths in alkali basaltic magma *at the time of xenolith incorporation* is presented, I believe it most reasonable to entertain the working hypothesis that the presence of ultramafic nodules in alkali basaltic volcanics is indicative of relatively high average flow rates. It is important to note that the conclusion reached here based on settling rate considerations is consistent with inferences based on kinetic considerations as cited earlier.

Propellant hypothesis

Introduction

If it is accepted that mafic alkalic magma moves upwards rapidly (cm/s to m/s), mechanisms for the mobilization of melt at depth must be sought. One hypothesis is that exsolution of volatile components provides the means for conversion of PV work into kinetic energy thereby accelerating magma upwards. A purpose of this paper is to determine the abundance of volatiles necessary for the propellant effect to be operative at sub-moho depths. A basic constraint is that upwelling xenolith-bearing magma needs sufficient kinetic energy to transport dense xenoliths from sub-moho depths.

In order to test the propellant hypothesis, I have derived and solved the conservation equations (continuity, momentum and energy) an appropriate equation of state for H_2O (Burnham et al. 1969; Sharp 1962; Helgeson and Kirkham 1974; Holloway 1977) and CO_2 (Shmonov and Shmulovich 1974; Holloway 1977; Flowers 1977; Spera and Bergman 1980; Kerrick and Jacobs 1981), a general equation of state for two phase (vapor plus vapor-saturated melt) mixtures and solubility expressions for H_2O (see Appendix II) and CO_2 (Spera and Bergman 1980) in mafic alkalic melts. Simultaneous solution of this coupled set of non-linear algebraic and ordinary differential equations enables the determination of the temperature (T), pressure (p), magma ascent rate (u), the composition of the vapor phase, the volatile content of the melt, and the mass fraction of vapor (ϕ) in the magma as a function of depth assuming closed system behavior. It is a relatively simple modification to allow for open system behavior by removing exsolved volatiles. Open-system behavior (i.e., removal of volatiles upon exsolution) has the effect of increasing magma density and viscosity and so that ascent of magma is impeded. In essence, the results of the calculations presented below tend to maximize magma ascent rates by assuming closed system behavior.

Because of the complexity of a crack network (see Shaw 1980; Hill 1977 for discussion of the topologic complexities of volcanic conduits, magma migration paths and fracture propagation in the lithosphere), it is necessary to one-dimensionalize the system. In a parametric sense, frictional losses in a complex conduit network can be roughly taken into account by estimating the effective friction coefficient (C_f). The normal friction factor (f) of incompressible viscous pipe flow is a measure of the skinfriction and conduit roughness only. The effect of constrictions, bends and crack tortuosity, is to increase frictional losses. In this study, the effects of additional head losses are accounted for by utilization of an effective friction coefficient, C_f. The additional flow resistance offered by constrictions and bends has been approximately estimated utilizing fluid dynamic empirical correlations such as those cited in Bird et al. (1960), or Shames (1982) and making simple assumptions regarding crack geometries.

Fluid-dynamic model of two-phase flow: deep ascent model

Homogeneous flow theory provides the simplest method for analyzing two-phase flow. Differences in velocity, temperature and chemical potential between the vapor and melt promote rapid exchange of momentum, heat and mass. In what follows, it is assumed that interphase transport phenomena proceed at high rates compared to ascent rates so that average values for the velocity, temperature, pressure and chemical potentials of CO_2 and H_2O in coexisting vapor and melt phases are identical. For steady homogeneous equilibrium flow in a constant area duct, the equations expressing conservation of mass, momentum and energy are (see Shapiro 1953; Wallis 1969; Spera 1981)

$$\frac{du}{dz} = -\frac{\dot{M}}{\rho^2}\frac{d\rho}{dz} \tag{1}$$

$$\frac{dp}{dz} = -\dot{M}\frac{du}{dz} - \frac{2C_f\dot{M}^2}{D}\frac{1}{\rho} - \rho g \tag{2}$$

$$\frac{dT}{dz} = \left(\frac{\bar{\alpha}T-1}{\rho\bar{C}_P}\right)\frac{dp}{dz} - \frac{u}{\bar{C}_P}\frac{du}{dz} - \frac{4B(T-T_w)}{\dot{M}D\bar{C}_P} - \frac{g}{\bar{C}_P} \tag{3}$$

Table 2. Parameters in Eq. (1) through (9)

u	vertical magma velocity
z	vertical coordinate
$\dot{M}$	mass flux, $\equiv \rho_i u_i$
p	magma pressure
C_f	effective friction coefficient
D	diameter of conduit
g	acceleration due to gravity
T	temperature
C_p	isobaric heat capacity of magma (see eq. 6b)
B	heat transfer coefficient (see eq. d, Appendix I)
Z_w^0	initial mass fraction of H_2O in the system
$Z_{CO_2}^0$	initial mass fraction of CO_2 in the system
X	mole fraction
$f_w^0, f_{CO_2}^0$	fugacity of pure H_2O and CO_2 at p, T

Greek symbols

ρ	density of two phase mixture (i.e., magma)
α	isothermal expansivity of magma (see eq. 6a)
ϕ	mass fraction vapor
β	isothermal compressibility
δ_w, δ_{CO_2}	see eqs. (4d and 4e)
θ_i	volume fraction of ith volatile species in the vapor phase
ξ	volume fraction of vapor in the magma

Subscripts and superscripts

w	wall or water
v	vapor
m	melt

Parameters appearing in Eqs. (1), (2) and (3) and those that follow in this section are defined in Table 2. Note that $\dot{M}$, the mass flux through the volcanic conduit (assumed to be a cylindrical pipe) is constant in steady flow and equal to $\rho_i u_i$ where ρ_i and u_i represent the density and velocity of magma as it leaves the reservoir. In order to close the system of equations, an equation of state for magma must be specified. The density of a magmatic mixture (ρ) is related to that of the vapor (ρ_v) and melt (ρ_m) phases by

$$\frac{1}{\rho} = \frac{\phi}{\rho_v} + \frac{(1-\phi)}{\rho_m} \tag{4a}$$

where ϕ is the mass fraction of the vapor phase in the two-phase mixture at a particular depth. In the general case, the vapor phase will be a multicomponent fluid. In this work a binary (H_2O-CO_2) vapor phase is considered. The vapor phase density is related to the composition of the vapor phase by

$$\frac{1}{\rho_v} = \frac{w_{CO_2}^v}{\rho_{CO_2}} + \frac{w_{H_2O}^v}{\rho_{H_2O}} \tag{4b}$$

where both ρ_{CO_2} and ρ_{H_2O} are functions of pressure and temperature and may be determined by evaluation of appropriate equations of state (refrences previously cited), and w_i^v represents the mass fraction of the ith component in the vapor phase. The density of the volatile-bearing melt phase is given by

$$\rho_m = \rho_0[1 + \beta_m(p - 10^5) - \alpha_m(T - 1473) + \delta_{H_2O}\, w_{H_2O}^m + \delta_{CO_2}\, w_{CO_2}^m] \tag{4c}$$

where ρ_0 is the density of devolatilized melt at 1,200° C and 10^2 k Pa (1 bar), and α_m and β_m represent the isobaric expansivity and isothermal compressibility of melt and are equal to 5×10^{-5} K^{-1} (Nelson and Carmichael 1979) and 7×10^{-11} Pa^{-1} (Stolper et al. 1981; Carmichael et al. 1977), respectively. The delta parameters, defined according to

$$\delta_{H_2O} \equiv \frac{1}{\rho_m}\left(\frac{\partial \rho_m}{\partial w_w^m}\right)_{T,\, p,\, w_{CO_2}^m} \tag{4d}$$

$$\delta_{CO_2} \equiv \frac{1}{\rho_m}\left(\frac{\partial \rho_m}{\partial w_{CO_2}^m}\right)_{T,\, p,\, w_w^m} \tag{4e}$$

are calculated from the data of Burnham and Davis (1971) and Spera and Bergman (1980) respectively and are taken as constants. Although δ_w, δ_{CO_2}, α_m and β_m are, strictly speaking, not constant, there are few experimental data to constrain their temperature and pressure dependence.

Because the vapor phase is a binary fluid, it is necessary to define a set of bulk vapor properties for the vapor solution. This, in general, is no simple matter as it involves the problem of non-ideal mixing in the system H_2O-CO_2. Although nonideal mixing in the vapor phase could be accounted for using the modified Redlich-Kwong equation of Kerrick and Jacobs (1981), in the present calculations ideal mixing in the binary vapor phase has been assumed for simplicity (e.g., see Eq. 4b). There is no conceptual difficulty in incorporating non-ideal mixing behavior into the numerical calculations. However, examination of activity – composition relations in the system H_2O-CO_2 as proposed by various investigators (e.g., Holloway 1977; Flowers 1977; Kerrick and Jacobs 1981) suggests that excess Gibbs Free energies of H_2O-CO_2 mixtures are fairly small at magmatic temperatures ($t \gtrsim 1{,}100°$ C) although accurate experimental data are extremely scarce at high pressure (i.e., p > 1.5 GPa).

Consistent with ideal mixing in the vapor phase the following mixing laws have been adopted in this study:

$$\alpha_v = \theta_w^v\, \alpha_w + (1 - \theta_w^v)\, \alpha_{CO_2} \tag{5a}$$

$$\beta_v = \theta_w^v\, \beta_w + (1 - \theta_w^v)\, \beta_{CO_2} \tag{5b}$$

$$C_{p,v} = w_w^v\, C_{p,w} + w_{CO_2}^v\, C_{p,CO_2} \tag{5c}$$

where θ_w^v represents the volume fraction of H_2O in the vapor phase.

Because the fluid dynamic model is based on the homogeneous flow assumption, it is necessary to define a mean isobaric expansivity and mean specific isobaric heat capacity of the two phase (vapor plus melt) mixture [see Eq. (3)]. These parameters are defined according to

$$\bar{\alpha} = \xi\, \alpha_v + (1 - \xi)\, \alpha_m \tag{6a}$$

and

$$\bar{C}_p = \phi\, C_{p,v} + (1 - \phi)\, C_{p,m} \tag{6b}$$

where ξ represents the volume fraction and ϕ, the mass fraction, of vapor in the two phase mixture (i.e., in the magma), respectively.

Equations (1), (2), (3), (4) represent four equations in the eight unknowns p, T, ρ, u, ϕ, w_w^v, w_w^m and $w_{CO_2}^m$ where the subscript w refers to H_2O component. In order to close this set of relations, two mass balance expressions and two thermodynamic solubility equations are specified. The mass balance equations follow directly from the assumption of

Table 3. Parameters for CO_2 solubility expression

Melt composition	$-A$	$-B$	$-C$
Kimberlite	7,800	7.4729	0.352
Nephelinite	8,200	7.4729	0.352
Alkali basalt	9,100	7.4729	0.352

The parameters A, B, C refer to Eq. (9) in text. At 1,400° C and 3 GPa (30 kbar), the concentration of CO_2 dissolved in melts of kimberlitic, nephelinitic and alkali basaltic composition are 11, 8.5 and 5 wt.% respectively for $X^v_{CO_2}=1$ (i.e., maximum CO_2 solubilities). It should be emphasized that the numerical constants in this table are based on very limited experimental data. $g(p, T)=-A/T-B-C(p-1)/T$

closed system behavior. They are:

$$Z^0_{H_2O}=\frac{18\,X^v_w\phi}{44-26\,X^v_w}+\frac{18\,X^v_w(1-\phi)}{18\,X^m_w+44\,X^m_{CO_2}+gfw(1-X^m_{CO_2}-X^m_w)} \quad (7)$$

$$Z^0_{CO_2}=\frac{44(1-X^m_w)\phi}{44-26\,X^v_w}+\frac{44\,X^v_{CO_2}(1-\phi)}{18\,X^m_w+44\,X^m_{CO_2}+gfw(1-X^m_{CO_2}-X^m_w)}. \quad (8)$$

Equations (7) and (8) fix the total amount of H_2O and CO_2 in the system. As magma ascends and decompresses, volatiles exsolve from the melt; the mass fraction of the vapor phase (ϕ) increases while X^m_w and $X^m_{CO_2}$ decrease. However, the total amount of H_2O and CO_2 in the system (vapor plus melt) remains constant and equals $Z^0_{H_2O}$ plus $Z^0_{CO_2}$, the initial volatile content of H_2O and CO_2 in the magma at the initiation of ascent.

The final equations needed to specify the state of the system are solubility expressions for H_2O and CO_2 as a function of p, T, f^0_w, $f^0_{CO_2}$ and X^v_w for particular bulk compositions. For all p and T, solubility equations modified from Spera and Bergman (1980) are used for CO_2. It should be noted that the experimental data upon which their expression is based are largely confined to high pressures ($p_{CO_2}\geqq 1$ GPa). Comparison of calculated values of $X^m_{CO_2}$ at low pressures ($p_{CO_2}\sim 200$ MPa) with extrapolations based on the data of Kadik et al. (1972) shows reasonably good agreement. Nevertheless, the solubility expression must be considered tentative because of the general lack of low pressure CO_2 solubility data. The solubility expression for CO_2 in alkalic mafic melt adopted here is

$$\ln X^m_{CO_2}-\ln(1-X^v_w)=\ln f^0_{CO_2}+g(p, T) \quad (9)$$

where $f^0_{CO_2}$ is the fugacity of pure CO_2 at p and T and the function g, which depends on p, T and melt composition, is defined in Table 3.

Considerably more information is available regarding the H_2O solubility in mafic melts as a function of pressure and temperature. Unfortunately, however, most experimental data are confined to $p<1$ GPa although some data do exist at higher pressures. In Appendix II, an expression for the H_2O content of alkalic basaltic melt as a function of p, T and f_w is derived for pressures up to 3 GPa and temperatures to about 1,400° C.

Computational algorithm

For magma at p and T and some initial volatile content (i.e., $Z^0_{H_2O}$ and $Z^0_{CO_2}$ prescribed) Eqs. (7)–(10) may be solved simultaneously to determine the mass and volume fraction of vapor (ϕ and ξ) and the equilibrium composition of coexisting vapor and volatile-saturated melt phases. Given some initial ascent velocity (u_i) Eq. (1)–(5) may then be solved numerically so that new values of p, T, u, ρ, etc. are determined. Values of all parameters may be calculated at each depth by iterative solution of the coupled system of algebraic and ordinary differential equations using a 4th-order Runge-Kutta algorithm (Carnahan et al. 1969). Standard numerical methods were employed to monitor and minimize truncation and round-off errors; no hint of numerical instability was noted in any of the simulations. The effective friction (C_f) and heat transfer (B) coefficients were calculated at each depth using empirically derived correlations (see Spera 1981, Appendix III). The effective friction coefficient is a function of crack roughness, the sum of all losses due to crack tortuosity (e.g. sudden changes in the conduit cross-sectional area) and the Reynolds number. The viscosity of the two phase mixture is used in the evaluation of Re. So long as $\xi<0.7$, melt is the continuous phase and the viscosity of the mixture lies in the range $0.1<\eta<10$ with η in Pa·s (Sibree 1934; Wallis 1969). If the magma minus lithostatic pressure falls below some small value (on the order of the tensile strength of peridotite, ~ 20 MPa) or the magma temperature falls below the local solidus, the run is terminated; a necessary condition for magma ascent is that $p>p_{lith}$ (Shaw 1980; Spera 1980) and $T>T_s$.

Results

Preamble and synopsis

The conclusions summarized below are based on the results of about 50 numerical experiments. The simulations were designed to systematically test the importance of magma bulk composition, initial conditions (e.g., mass flux, initial depth), heat transfer coefficient (B), lumped friction factor (C_f), conduit diameter, H_2O/CO_2 ratios, the local geothermal gradient, and different melt bulk compositions on the dynamic evolution of ascending magma. Clearly, the simulations are approximations to a complex set of interrelated dynamic and thermal phenomena. However simplified the one-dimensional pseudofluid model may be, the inclusion of terms accounting for: (1) mechanical and thermal irreversibilities, (2) measured PVT and thermal properties of H_2O and CO_2 and (3) an equation of state for the melt that explicitly accounts for the effects of p, T and volatile concentration on melt density, offers some hope that the model is not overly simplified. The simulations reported here extend and amplify the earlier results of McGetchin and Ullrich (1973) and Lang (1972).

It should also be emphasized that this report focuses on the "deep ascent" part of the decompression path. Specifically, the expansion behavior at depths less than 3 km is not explicitly discussed. Although solutions were obtained along the entire ascent path (i.e., to the surface), a flow transition occurs at shallow depths ($Z\sim 3$ km). Physically this transition corresponds to the high rate of change of the isothermal compressibility of volatile-saturated magma at low pressure. This thermodynamic feature is manifested dynamically as a change from low speed quasi-

Table 4. Kimberlite

Initial conditions

Run No.	Z_i (km)	T_i (° C)	P_i (GPa)	U_i (m/s)	$\dot{M}$ (kg/m²s)	D (m)	B (J/m²s)	C_f	Z_w^0 (wt.%)	$Z_{CO_2}^0$ (wt.%)	ϕ (wt.%)	W_w^m (wt.%)	$W_{CO_2}^m$ (wt.%)	X_w^v (mole frac.)
6	80	1,400	2.4	24	5.9×10^4	30	3×10^3	0.0825	10	10	6.4	8.9	5.6	0.46
10	80	1,400	2.4	24	5.9×10^4	30	5×10^3	0.0825	2	18	10.5	2.0	8.6	0.05
16	80	1,400	2.4	10	2.4×10^4	5	0	0.0138	10	10	6.4	8.9	5.6	0.46
21	80	1,400	2.4	24	5.8×10^4	30	2×10^3	0.0825	18	2	2.9	1.4	16.3	0.89
24	150	1,400	4.7	24	4.2×10^4	30	2×10^3	0.0825	20	20	9.4	19.4	14.4	0.46
26	150	1,400	4.7	24	5.2×10^4	30	2×10^3	0.120	20	20	9.4	19.4	14.4	0.46
30	150	1,400	4.7	24	5.2×10^4	30	2×10^3	0.132	20	20	9.4	19.4	14.4	0.46
Alkali Basalt														
37	80	1,400	2.4	1.2	3.3×10^3	5	0	0.5	5	5	1.8	4.9	3.5	0.21
38	80	1,400	2.4	2	6.6×10^3	5	0	0.5	5	5	1.8	4.9	3.5	0.21
39	80	1,400	2.4	2.5	7×10^3	5	0	0.5	5	5	1.8	4.9	3.5	0.21
B	80	1,400	2.4	2.5	6×10^3	5	0	0.5	10	10	10.0	8.4	2.7	0.44
D	80	1,400	2.4	2.5	7×10^3	5	10^2	0.5	5	5	1.8	4.9	3.5	0.21
J	120	1,400	3.7	2.5	6.67×10^3	5	10	0.75	2	18	12.8	2.0	6.3	0.05
K	120	1,400	3.7	2.5	6.67×10^3	5	10^2	0.85	2	18	12.8	2.0	6.3	0.05

Parameters at 3 km depth

Run No.	P (MPa)	T (° C)	U (m/s)	ρ (kg/m³)	ϕ (wt.%)	ξ (vol%)	X_w^v (mole frac.)
6	124	1,283	60	989	17	70	0.64
10	84	1,180	62	959	19	76	0.13
16	621	1,351	12.6	1,942	13.6	36	0.54
21	160	1,320	62.4	930	21	76	0.96
24	834	1,326	35.2	1,473	34	62	0.65
26	295	1,445	56.8	914	36.3	78.6	0.67
30	Magma stagnates at $Z=10$ km						
37	413	1,353	1.5	2,270	5.7	20	0.37
38	306	1,382	2.6	2,164	6.0	25	0.41
39	213	1,406	3.5	2,004	6.4	33	0.45
B	511	1,384	3.3	1,839	14.5	41	0.55
D	Magma stagnates at $Z=5$ km						
J	368	1,404	3.8	1,754	18.2	0.49	0.08
K	Magma stagnates at 35 km						

incompressible flow ($M \lesssim 0.2$) to transonic compressible flow ($M \sim 1$), where M is the Mach number. It is commonly observed that conduit cross-sectional areas increase (e.g. the classic funnel-shaped diatreme structure) in the near surface environment. This factor enhances the compressibility effect in driving a low speed subsonic flow towards transonic behavior. However, in the "deep seated" environment, essentially nothing is known regarding the variation of conduit cross-sectional area with depth. Therefore, to keep the model as simple as possible, conduits are assumed to remain constant in width.

Detailed results for some of the numerical experiments are given in tabular form in Tables 4 and 5. Rather than discuss each simulation separately or any one simulation in particular, general comments emphasizing the most sensitive parameters governing the ascent trajectory are given in the following sections. Most of the simulations listed in Tables 4 and 5 were purposely carried out starting with rather high initial H_2O and CO_2 contents. Examination of final velocities shows that even for such high initial concentrations of volatiles, the fractional change in vertical velocity ($\Delta u/u_i$) is less than or equal to about 2. A main conclusion of this study, therefore, is that in deep-seated environments the exsolution of volatiles leads to a rather *small* increase in magma ascent rate. The exsolution of dissolved volatiles does not "explosively" accelerate magma through the lithosphere. This is not to say that volatiles play no role in the ascent process, but only that ascent rates do not vary over orders of magnitude between the source and the near-surface. In this view, kimberlitic or alkali basaltic melt does not segregate from a peridotitic source and then move upwards slowly as a km-sized magma diapir. Instead the following scenario is envisioned. A relatively small volume of peridotitic mantle undergoes partial fusion to a limited extent (1 to 10%). The ultimate cause of fusion may be pressure-release melting or perhaps fusion is triggered by the infiltration of MMF with attendant heat transfer (Spera 1981). In any case magma pressure within the partial melt region gradually rises above the mean normal stress due to the volume increase upon fusion. When the magma minus mean normal stress rises above some critical value (of order 30 MPa) a crack (or number of cracks) nucleates and magma impulsively surges upwards at cm/s to m/s.

A recent analysis by Spence and Turcotte (1984b) shows that long cracks (1 to 10^2 km) of narrow width (0.1 to 5 m) will propagate at m/s rates when driven by slightly pressured magma ($p - p_{lith} \sim 5$ to 50 MPa). Their model is complementary to the one developed here in that it shows that, indeed, fractures of appropriate size will form and propagate at requisite rates. In the purely fluid dynamic model presented here, fractures are assumed to exist *a priori*. There is, therefore, no need to call upon a "propellant" effect to explain alkalic magma ascent rates through the lithosphere. As noted previously (Spera 1980), a modest vertical effective stress gradient will drive low viscosity (0.1 to 10^2 Pa s) magma upwards at cm/s to m/s rates. The critical factor is the absolute value of the mean normal effective stress (defined here as $\sigma_0 - p$, where p is the magma pressure and σ_0 is the mean normal stress) at the initiation of magma ascent (Fowler 1984).

Table 5.

Depth (km)	T (° C)	P (MPa)	U (m/s)	ρ (kg/m^3)	ϕ (%)	ξ (vol %)	X_w^v (mole frac.)	$w_{CO_2}^w$ (wt.%)	$w_{H_2O}^m$ (wt.%)	M Mach Number
Run No. 6										
80	1,400	2,428	24.0	2,446	6.4	13.7	0.46	5.6	8.9	0.0094
70	1,412	2,112	24.6	2,391	7.3	15.7	0.46	5.0	8.7	0.0097
60	1,416	1,800	25.2	2,332	8.4	18.3	0.47	4.2	8.5	0.0102
50	1,414	1,492	25.9	2,265	9.6	21.4	0.48	3.4	8.2	0.0111
40	1,405	1,190	26.9	2,183	10.9	25.2	0.50	2.5	7.7	0.0126
30	1,388	890	28.2	2,076	12.1	29.9	0.52	1.7	7.1	0.0156
20	1,362	600	30.6	1,915	13.7	37.4	0.55	1.0	6.4	0.0222
15	1,345	457	32.8	1,788	14.4	41.5	0.56	0.7	5.8	0.0289
10	1,324	318	36.8	1,593	15.3	50.8	0.59	0.4	5.2	0.0421
5	1,297	180	47.4	1,238	16.4	61.8	0.62	0.2	4.2	0.077
3	1,283	124	59.4	988	17.0	70.6	0.64	0.1	3.5	0.115
Run *D*										
80	1,400	2,428	2.5	2,797	1.8	4.1	0.21	3.5	4.9	0.001
70	1,398	2,121	2.55	2,739	2.3	5.4	0.21	3.0	4.9	0.0011
60	1,385	1,819	2.61	2,682	3.0	7.0	0.22	2.4	4.8	0.0011
50	1,363	1,522	2.66	2,625	3.6	8.8	0.23	1.8	4.8	0.0011
40	1,331	1,230	2.73	2,565	4.3	10.6	0.25	1.3	4.7	0.0012
30	1,289	942	2.7	2,499	4.9	12.7	0.28	0.8	4.6	0.0013
20	1,236	661	2.9	2,419	5.5	15.5	0.31	0.4	4.4	0.0016
15	Magma freezes									

Effects of initial conditions, friction and heat-transfer coefficients

Although all parameters have a demonstrable effect on the ascent path, the initial conditions, frictional and heat-transfer factors play the dominant role. For example, an increase in C_f by a factor of two increases the depth of magma stagnation from 5 km to 25 km for a kimberlitic magma with 20 wt.% volatiles ($Z^0_{H_2O}=0.1=Z^0_{CO_2}$) starting ascent at 80 km (2.3 GPa) where $T_i=1{,}400°$ C with B, the heat-transfer coefficient, equal to 2×10^3 J/m^2 s K. This behavior is easily rationalized by inspection of Eq. 2. Similarly, for constant C_f equal to 0.08 and 25 wt.% volatiles, the magma temperature at a depth of 3 km equals 1,400° C, 1,280° C or 1,175° C for B equal to 0, 3×10^3 J/m^2 s K or 6×10^3 J/m^2 s K respectively. As noted previously, magma ascent is arrested when either $p<p_t$ or T falls below the local solidus temperature. Failure of magma to reach the surface in any simulation could always be traced to one of these causes. Examination of Eq. (2) reveals that $\dot{M}$, the steady state mass flux through the conduit, plays a significant role in regulating the head loss during ascent. Note that $\dot{M}$ is imposed as an initial condition and that the pressure loss is proportional to $\dot{M}^2$. For adiabatic ascent ($B=0$), a high initial mass flux correlates with both high head loss and the initial rate of magma acceleration. This effect follows from the non-linear coupling between Eqs. (1), (2) and (4). Maximum velocities are achieved when the magma pressure approaches the local lithostatic pressure. If $\dot{M}$ is very large however, the magma pressure will fall below lithostatic and the conduit cannot remain open (magma ascent arrested). In non-adiabatic flows ($B>0$), a large value of $\dot{M}$ will decrease the importance of heat losses to the surrounding lithosphere and therefore promote ascent. In summary, the impossibility of making any sweeping generalizations by causual inspection of the coupled and non-linear set of equations governing ascent is emphasized. Seemingly paradoxical results such as a slight increase in magma velocity for an increase in the friction factor are, in fact, to be expected in light of the strongly nonlinear nature of the coupling between the field variables appearing in the conservation, solubility and PVT relations. Finally, it is worth repeating that many simulations ended with magma stagnation at depth. This suggests that mantle metasomatism may be a rather widespread phenomenon especially in cold subcontinental lithosphere where non-adiabatic ascent may be common.

The depth from which ascent begins has an effect on ascent dynamics because of several interrelated factors. For constant C_f and B, head and heat losses will be greater for flows originating at deeper depths. On the other hand, the deeper the initial depth, the greater the volatile content (at saturation) of magma and so buoyancy forces are maximized. Detailed calculations indicate that depth of origin has relatively little influence on the velocity of magma at any depth. Significantly, however, for low speed flows with small frictional and heat losses (i.e., C_f and B are small) magma arrives in the near-surface environment significantly overpressured. That is, although the local velocity is not particularly high, the *potential* for near surface transonic behavior is enhanced over the case where Z_i is smaller. This seems consistent with differences between inferred ascent rates for kimberlites (fast) and garden-variety alkali basalts which transport spinel peridotite xenoliths.

Role of volatiles

The next most important parameter relates to the initial volatile content of magma at its source. The distribution of CO_2 and H_2O between the melt and vapor is governed by equilibrium thermodynamics and so the mass fraction of the vapor phase (ϕ) at the initiation of ascent depends on the bulk H_2O/CO_2 ratio as well as their absolute abundances. As is well-known, H_2O is far more soluble than

CO_2 in basaltic melts. In kimberlite melts, CO_2 solubilities may approach (or even exceed) H_2O contents at high pressures ($P_t > 3$ GPa) where melt compositions become carbonatitic (Wyllie 1980; Eggler 1978). We have not attempted simulation of carbonatitic ascent here although the algorithm could easily be modified to accommodate such an extreme magma composition. Because CO_2 vapor is denser than H_2O at any P_t and T, CO_2-rich magma is less overpressured compared to H_2O-rich ones at a given depth, other parameters being fixed (e.g., C_f, B, D, Z_i, geothermal gradient, etc.). This implies that H_2O is a better propellant (per unit mass) as it is the conversion of PV work into kinetic energy that accelerates magma upwards. The different PVT properties of a CO_2 versus H_2O-rich vapor phase leads to modest differences in magma temperatures at a given depth other parameters being fixed. As pointed out previously (Spera 1981), irreversible expansion of a non-ideal fluid can lead to either heating or cooling of that fluid due to a non-zero Joule-Thompson coefficient. The PVT properties of CO_2 (Spera and Bergman 1980; Kerrick and Jacobs 1981) are such that irreversible decompression at magmatic temperatures is always accompanied by *heating* of the fluid. H_2O, on the other hand, has a Joule-Thompson inversion pressure of about 0.3 GPa (3 kb) at magmatic temperatures and consequently *cools* upon irreversible decompression for $Z < 12$ km. This phenomenon explains the reason why (with all other factors being equal) a CO_2-rich magma remains slightly hotter than a corresponding H_2O-rich one at any given depth. For instance, an alkalic magma with 10 wt.% CO_2 (i.e., $Z^0_{CO_2} = 0.1$, $Z^0_{H_2O} = 0$) arrives near the surface at temperatures about 30° C higher than one containing 10 wt.% H_2O and no CO_2. In this same simulation $\delta u/u$, a parameter that measures the acceleration of the fluid, is about 1.8 for the CO_2-rich magma versus 2.5 for the H_2O rich one at $Z = 3$ km. Given an initial magma velocity of 1 m/s, the velocity at 3 km depth is about 3 m/s for the CO_2-rich melt and 4 m/s for the H_2O-rich melt. Note that the speed of the magma is only a little greater than its initial value. This is a general feature of all the simulations carried out in this study. The so-called propellant effect is actually quite unimportant. It follows from this that the inferred high rate of ascent of alkaline versus tholeiitic magma has more to do with initial conditions than it does with the propellant effect *per se*. This is not to say that volatiles are not important to the dynamics of ascent. Indeed, initial ascent rates are presumably governed by the mechanics of crack propagation. Rates of "brittle" failure in turn depend on the chemical environment, pressure distribution and magma viscosity at the tip of the propagating crack (Anderson 1979; Spence and Turcotte 1983; Stevenson 1983). Each of these factors depend upon the volatile content of the magma. To first order, the initial ascent rate of magma from a reservoir will correlate with the magma over-pressure at the instant of reservoir failure. As noted previously (Spera 1980, 1981, 1982), magma overpressures need not be very large (few tens of bars) in order to drive magma upwards at an appreciable rate. In this view, the source region of MORB is too hot and volatile-poor to allow for initial ascent rates greater than a few cm/s. In fact, the strength of the peridotitic matrix may be essentially zero and therefore the initiation of ascent is more a problem in percolation theory than in reservoir-failure mechanics. In distinction, however, a relatively cold portion of say sub-continental lithosphere or old oceanic lithosphere may be sufficiently strong to set up a pressure-cooker effect so that at the time of reservoir failure magma is overpressured enough to quickly accelerate to velocities around several m/s.

Summary and conclusions

In Table 5 detailed paths are presented for two typical cases. Run 6 models an ascending kimberlite whereas Run *D* is applicable to alkali basalt migration. The two ascent trajectories qualitatively encapsulate the kinds of behavior found in the numerical experiments. Magma following the path of Run 6 successfully breaches the surface whereas in Run *D*, magma stagnates within the upper part of the lithosphere due to significant heat losses.

The main conclusions of this study may be summarized as follows:

(1) In most circumstances, ascent rates and conduit diameters are small enough and local lithospheric temperature low enough so that the *assumption* of adiabatic (i.e., $B = 0$) flow is generally a poor one especially when magma traverses old (cold) lithosphere. In other words, when the ratio of heat transport rate by vertical advection to diffusion is not sufficiently large, the conduit is narrow and the ambient lithospheric temperature low, rising magma will suffer heat death.

(2) Alkaline magma travels through the mantle in swarms of propagating magma-filled cracks rather than as large buoyant diapirs. Crack propagation rates and stress-intensity factors are known to depend on the activity of volatile components. It is through a crack propagation mechanism rather than purely fluid dynamic mechanism (volatile exsolution) that volatiles play an important role in the transport of alkaline magma through the deep lithosphere.

(3) Mantle metasomatism is a natural consequence of the non-adiabatic ascent of magma in narrow (meter-sized) conduits through the lithosphere. The composition of mantle metasomatic fluid is determined by the initial volatile content of the magma and the stability of hydrous and carbonate-bearing phases. The very common occurrence of nearly pure CO_2 fluid inclusions in mantle xenoliths reflects the instability of carbonates relative to OH-bearing phases (e.g. amphiboles, phlogopite, apatite). Note that the latter phases are common in modally metasomatized peridotites whereas the carbonates are rarer.

(4) The velocity of ascending magma is governed by a balance amongst pressure, buoyancy and viscous forces; inertial forces are not very important even for very volatile-rich magma because of the relatively small compressibility of H_2O and CO_2 at $P_t > 100$ MPa. The main role volatiles play in the deep ascent process is in controlling the dynamics at the initiation of ascent and in determining the local magma pressure.

(5) Inferences on ascent rates based on various kinetic constraints suggest typical velocities in the range 10^{-1} to several m/s for alkali basalts and 10 to 30 m/s for kimberlites in deep-seated environments.

(6) In the near-surface environment essentially all magmas attain volatile-saturation. Coupled with the enormous increase in volatile-phase compressibility this effect drives magma to transonic speeds. Rheological properties of two phase (melt plus vapor) magmatic suspensions are vastly

different in the transonic regime (Wilson et al. 1980; Housley 1978).

Appendix I: Simple thermal model

When magma travels through a narrow (few meters) conduit within the lithosphere, the flow may be markedly non-adiabatic. The precise amount of heat transfer between magma and country rock depends on the conduit geometry (diameter and surface area), magma ascent rate, the lithospheric temperature distribution and the viscosity temperature relationship for magma. Calculations by Delaney and Pollard (1982) indicate that within the upper crust basaltic magma ascends only a few kilometers before complete solidification when moving, for example, in a 2 m diameter conduit at 1 m/s. Here it is of interest to examine the situation for magma transport through the deeper lithosphere. Because of potentially greater transport distances it is important to consider the effects of the geothermal gradient on heat transfer. The calculations presented here show that for typical geometric, transport and dynamic parameters, transport distances are on the order of a few tens of kilometers.

It is assumed that magma flows upwards at a mean velocity u through a cylindrical pipe of diameter D. The temperature of magma at the "inlet" is T_i; the lithospheric temperature distribution is approximated by an expression of the form

$$T_{CR}=k_1+k_2\,h^{1.5} \tag{a}$$

where k_1, k_2 are constants and h represents the height above the magma inlet (i.e., $T=T_i=T_{CR}$ at $h=0$, where T_{CR} is the local country rock temperature). A simple analytical model based on the local heat-transport factor (B) and a spatially variable conduit wall temperature, $T_w(z)$ leads to the expression (e.g., Kay 1968; Rohsenow and Choi 1962).

$$\frac{T-T_w(z)}{T_i-T_w(z)}=\exp\left(\frac{-4BZ}{k\,\mathrm{Pe}}\right) \tag{b}$$

where T, k and Pe represent the radially averaged magma temperature, magma thermal conductivity and peclet number respectively. The Peclet number is defined according to

$$P_e=\frac{\rho C_p\,uD}{k} \tag{c}$$

Empirical and analytical heat transfer studies are conveniently summarized by a heat-transfer coefficient valid for laminar viscous flow of a newtonian melt

$$B=\frac{1.86\,k}{D}\left(\frac{\mathrm{Pe}}{Z}D\right)^{1/3}\left(\frac{\eta_T}{\eta_{T_w}}\right)^{7/50} \tag{d}$$

when η represents the apparent viscosity. It should be noted that (d) is an empirical correlation for the heat transfer coefficient B. Most of the data Eq. (d) is based upon refer to isoviscous flow; the viscosity correction term is only valid for small values of a $(T_{CR}-T)$. However, in the present parameterized model, the temperature at any depth is the radially averaged one; no information regarding the spatial variation of T can be derived from this simplified model. To the extent that crystallization occurs along the margins of the conduit, the effective heat transfer coefficient for the flow will decrease. On the other hand, when marginal crystallization occurs, the diameter of the conduit will decrease and this tends to increase the heat transfer coefficient. For a viscosity law applicable to magma at subliquidus temperatures we take (Shaw 1969; Delaney and Pollard 1982; Feigenson 1981; Spera et al. 1982)

$$\eta=\eta_{T_w}\exp\left(a(T_r-T)\right) \tag{e}$$

The viscosity ratio in (d) therefore becomes

$$\frac{\eta_T}{\eta_{T_w}}=\exp(a(T_w-T)) \tag{f}$$

When Eqs. (c), (d) and (f) are substituted into (b) an expression for the mean magma temperature as a function of height above and inlet depth may be determined. That is

$$T=\frac{T_{CR}(1-\exp\alpha)+2T_i\exp\alpha}{1+\exp\alpha} \tag{g}$$

where the depth-variable conduit wall temperature is taken as

$$T_w=\frac{T_{CR}+T}{2} \tag{h}$$

and α is defined according to

$$\alpha=-7.44\left(\frac{Z}{\mathrm{Pe}D}\right)^{2/3}\exp\left(0.075a(T_{CR}-T)\right). \tag{i}$$

Equation (g) gives the dependence of mean magma temperatures on all relevant physical parameters (e.g., peclet number, conduit size, magma properties, geothermal gradient, etc.). For reference it is noted that the liquidus temperature for basalt drops about 4° per kilometer in vapor-absent conditions. In many cases (see Fig. 1) the temperature decrement due to heat transfer exceeds the liquidus temperature gradient. It is noted therefore that heat death may be a common occurrence for magma ascent through the lithosphere.

Appendix II: Solubility of H_2O in melts

The most comprehensive and internally consistent set of experimental H_2O solubility ($p_t-T-X_w^m-V_w^m$) data for silicate melts are those of Burnham and coworkers (Burnham and Davis 1971, 1974) for H_2O in melts of albitic composition. Although numerous additional data on equilibrium H_2O contents for natural melts exist (see Nicholls 1980 for a partial review), very few data are available for $p_t>1$ GPa and only rarely have investigators exploited $p_t-T-X_w^m$ data for retrieval of partial molar volume data for H_2O in melts at elevated temperatures and pressures (e.g., Hodges 1974).

In order to determine internally consistent thermodynamic expressions for the solubility of H_2O in mafic melts under a wide range of physical conditions ($1{,}000<t<1{,}500$° C, $0<p_t<3.2$ GPa) we have critically compiled a primary set of solubility data from a number of sources (Khitarov et al. 1959; Burnham and Jahns 1962; Hamilton et al. 1964; Spengler and Burnham 1966; Burnham and Davis 1971, 1974; Scarfe 1973; Shaw 1974; Oxtoby and Hamilton 1978; Hodges 1974; Eggler and Kadik 1979; Stern and Wyllie 1973; Boettcher and Wyllie 1969; Kadik and Lebeder 1969). Although some of these data are inconsistent, it does prove possible to derive smoothed values for the chemical potential of H_2O in basaltic melt within the entire $p_t-T-w_w^m$ range of petrologic importance. Fortunately, the effect of melt composition on equilibrium H_2O content appears small; H_2O solubility correlates only weakly with silica and alkali oxide activities for the range of compositions relevant to naturally occuring melts especially at high pressure. The expressions below specifically apply to melt of basaltic composition although they recover solubility data for $NaAlSi_3O_8$ melt fairly well.

The solubility of H_2O in a melt is governed by the soichiometric heterogeneous equilibrium relation

$$H_2O_{(m)} \rightleftharpoons H_2O_{(v)} \tag{1}$$

For our purposes the distribution of H_2O between molecular water and hydroxyl is immaterial; we are concerned only with the *total* amount of water that dissolves in the melt (Stolper 1982). We treat the non-ideal behavior of H_2O in a melt in terms of strictly regular solution theory. For reaction (1) thermodynamic equilibrium necessitates that

$$\ln f_w-2\ln X_w^m=\frac{D}{T}(1-X_w^m)^2+A/T+B+C\ln T+\int_0^P\frac{\bar{V}_w^m}{RT}\,dP \tag{2}$$

where the following assumptions have been made:

a) H_2O-melt mixing can be described by strictly regular solution theory

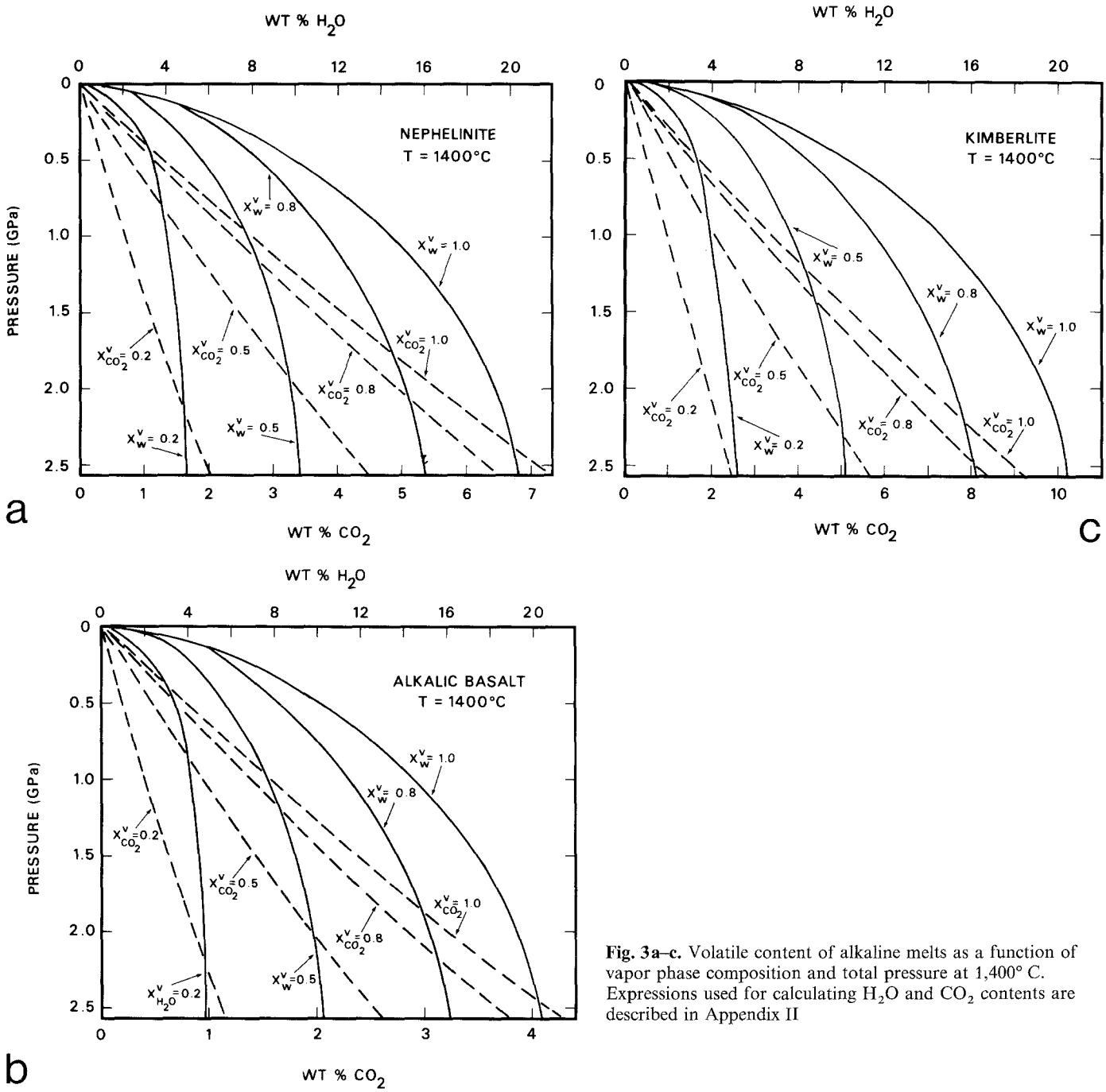

Fig. 3a–c. Volatile content of alkaline melts as a function of vapor phase composition and total pressure at 1,400° C. Expressions used for calculating H_2O and CO_2 contents are described in Appendix II

b) ΔC_p^0 of reaction (1) is constant

c) Henry's Law in the form $f_w = k(X_w^m)^2$ is valid in the limit $X_w^m \to 0$.

d) $\bar{V}_w^m$, the partial molar volume of H_2O dissolved in the melt, is independent of composition.

It may be mentioned that an attempt was made to fit the solubility data to an expression similar to (2) except that the form for Henry's Law was modified to $f_w = k' X_w^m$. This resulted in a fit that was statistically poorer than one based on assumption (c). The last term on the RHS of (2) was assumed to be of the same form (but different numerical values) as given by Burnham and Davis (1971) for H_2O in $NaAlSi_3O_8$ melt. That is,

$$\int_0^P \frac{\bar{V}_w^m}{RT} dP = \left(\frac{a_1}{T} + a_2 + a_3 T + a_4 T^2\right) P + \left(\frac{a_5}{T} + a_6 + a_7 T\right) P^2 + \left(\frac{a_8}{T} + a_9\right) P^3 + \frac{a_{10}}{T} P^4. \quad (3)$$

Regression of the smoothed set of H_2O solubility data was performed by the usual numerical techniques. Numerical values of the parameters D, A, B, C and a_i where i=1 to 10 are listed in Table 6. Retrieval of thermodynamic parameters utilized the H_2O fugacity data of Burnham et al. (1969) for $P_t < 1$ GPa and that listed in Spera (1974) for $P_t > 1$ GPa. In practice, modified Redlich-Kwong equations of state for H_2O were used over narrow $P_t T$ ranges to facilitate numerical calculations. Solubility relations as a function of temperature, pressure and vapor phase composition are summarized in Fig. 3.

Acknowledgements. This research was supported by grants from the National Science Foundation EAR-81-21200 and EAR-81-15728. A grant from the Princeton University Computer Center greatly facilitated the numerical simulations reported herein. Critical reviews by E. Stolper and J. Nicholls greatly improved the form and content of this work. D. Turcotte and A. Fowler made

Table 6. Parameters for H_2O solubility calculations

$D = 2438.6$	$A = -1612.7$	$B = 1.0775$
$C = 1.2927$	$a_1 = -0.53455$	$a_2 = 1.418 \times 10^{-3}$
$a_3 = -7.639 \times 10^{-7}$	$a_4 = 1.354 \times 10^{-10}$	$a_5 = 6.0477 \times 10^{-6}$
$a_6 = -1.95 \times 10^{-8}$	$a_7 = 6.474 \times 10^{-12}$	$a_8 = 2.648 \times 10^{-10}$
$a_9 = 1.397 \times 10^{-14}$	$a_{10} = -3.525 \times 10^{-15}$	

Regression parameters are consistent with temperature in Kelvin, pressure and fugacity in bars. The mole fractions of H_2O and CO_2 in the melt are related to corresponding mass fractions by the following

$$w_w^m = \frac{18 X_w^m}{18 X_w^m + 44 X_{CO_2}^m + gfw(1 - X_{CO_2}^m - X_w^m)}$$

$$w_{CO_2}^m = \frac{44 X_{CO_2}^m}{18 C_w^m + 44 X_{CO_2}^m + gfw(1 - X_{CO_2}^m - X_w^m)}$$

The gfw is defined according to $gfw = \Sigma_i X_i M_i$ where X_i and M_i represent the mole fraction and molecular weight of the ith component in the melt where H_2O and CO_2 have not been included

preprints available. D. Yuen is gratefully acknowledged for helpful commentary and active interest in this project. The thermal crisis hotline number is (602)965–5081. Ask for John Holloway. Jayne Bialkowski flawlessly typed the manuscript innumerable times and drafted the figures

References

Aki K, Koyanagi R (1981) Deep Volcanic tremor and magma ascent mechanism under Kilauea, Hawaii. J Geophys Res 86:7095–7109

Aki K, Fehler M, Das S (1977) Source Mechanism of volcanic tremor: Fluid-driven crack models and their application to the 1963 Kilauea eruption. J Volcanol Geotherm Res 2:259–287

Anderson OL (1979) The Role of Fracture Dynamics in kimberlite pipe Formation. In: Boyd FR, Meyer HOA (eds) Kimberlites, Diatremes, and Diamonds: Their Geology, Petrology and Geochemistry. Am Geophy Union

Arculus RJ (1975) Melting behavior of two basanites in the Range 10 to 35 Kbar and the effect of TiO_2 on the olivine-diopside reactions at high pressures. Carnegie Inst Wash Yearb 74:512–515

Bailey DK (1982) Mantle Metasomatism – continuing chemical change within the Earth. Nature 296:no. 5857:525–530

Bergman SC (1982) Geochemistry, Petrology and Geology of the Lunar Crater Volcanic Field, unpublished dissertation (Ph.D.). Princeton University, Princeton, NJ

Best MG (1974a) Mantle derived amphibole within inclusions in alkali basaltic lavas. J Geophys Res 79:2107–2113

Best MG (1974b) Contrasting types of Cr-spinel peridotite xenoliths in basanitic lavas, W. Grand Canyon, Arizona. Earth Planet Sci Lett 23:229–237

Best MG (1970) Kaersutite – peridotite inclusions and kindred megacrysts in basanitic lavas, Grand Canyon, Arizona. Contrib Mineral Petrol 27:25–44

Bird RB, Stewart WE, Lightfoot EN (1960) Transport Phenomena, John Wiley, New York

Boettcher AL, O'Neil JR (1980) Stable isotope, chemical and petrographic studies of high-pressure amphiboles and micas: Evidence for metasomatism in the mantle source regions of alkali basalts and kimberlites. Am J Sci 280-A:594–621

Boettcher AL, O'Neil JR, Windom KE, Stewart DC, Wilshire HG (1979) Metasomatism of the Upper Mantle and the Genesis of Kimberlites and alkali basalts. In: Boyd et al. (eds) The Mantle Sample: Inclusions in Kimberlites and other Volcanics. Int Kimb Con, Am Geophys Union

Boettcher AL, Wyllie PJ (1969) Phase relationships in the system $NaAlSiO_4 - SiO_2 - H_2O$ to 35 Kb. pressure. Am J Sci 267:875–909

Burnham CW, Davis NF (1974) The role of H_2O in silicate melts: II. Thermodynamic and phase relations in the system $NaAlSi_3O_8 - H_2O$ to 10 kilobars, 700° C to 1,000° C. Am J Sci 274:902–940

Burnham CW, Davis NF (1971) The role of H_2O in silicate melts I. $P-V-T$ relations in the system $NaAlSi_3O_8 - H_2O$ to 10 kilobars and 1,000° C. Am J Sci 270:54–79

Burnham CW, Holloway JR, Davis NF (1969) Thermodynamic properties of water to 1,000° C and 10,000 bars. Geol Soc Am Spec Pap 132:pp 96

Burnham CW, Johns RH (1962) A Method for determining the solubility of water in silicate melts. Am J Sci 260:721–745

Carmichael ISE, Nicholls J, Spera FJ, Wood BJ, Nelson SA (1977) High Temperature properties of silicate liquids: applications to the equilibration and ascent of basic magma. Phil Trans R Soc London A 286:373–431

Chapman NA (1976) Inclusions and Megacrysts from under saturated Tuffs and Basanites, East Fife, Scotland. J Petrol 17:472–498

Carnahan B, Luther HA, Wilkes JO (1969) Applied Numerical Methods. J Wiley, New York, pp 604

Cohen LH, Ito K, Kennedy GC (1967) Melting and phase relations in an anhydrous basalt to 40 kilobars. Am J Sci 265:475–518

Cooper JA, Green DH (1969) Lead isotope measurements on lherzolite inclusions and host basanites from Western Victoria, Australia. Earth Planet Sci Lett 6:69–76

Crisp J (1983) Rates of Magmatism. J Volcanol Geotherm Res 20:177–211

Delaney PT, Pollard DD (1982) Solidification of basaltic magma during flow in a dike. AJS 282:856–885

Eggler DH, Kadik AA (1979) The system $NaAlSi_3O_8 - H_2O - CO_2$ to 20 Kbar pressure: I Compositional and Thermodynamic relations of liquids and vapors coexisting with albite. Am Mineral 64:1036–1048

Eggler DH (1978) The effect of CO_2 upon partial melting of peridotite in the system $Na_2O - CaO - Al_2O_3 - MgO - SiO_2 - CO_2$ to 35 kb, with an analysis of melting in a peridotite-$H_2O - CO_2$ system. Am J Sci 278:305–343

Eggler DH (1974) The effect of CO_2 on the melting of peridotite. Carnegie Inst Wash Yearb 73:215–224

Feigenson M, Spera FJ (1981) Technique for the rheologic study of high-viscosity melts. EOS Trans Am Geophys Union (abstr) 67:426–427

Feigenson M (1981) Aspects of the petrology of Oceanic basalts: I Geochemistry of Kohala Volcano, Hawaii. II. Petrochemistry of sea-floor basalts associated with Manganese ores from California. III. Rheology of Subliquidus basalts and other Silicate melts. Ph.D. Dissertation, Princeton University, Princeton, NJ

Flowers G (1977) Correction of Holloway's (1977) Adaption of the Modified Redlich-Kwong Equation of State for Calculation of the fugacities of Molecular Species in Supercritical fluids of Geologic interest. Contrib Mineral Petrol 69:315–318

Fowler AC (1984) A mathematical model of magma transport in the asthenosphere, preprint

Freund F, Kathrein H, Wengeler H, Knobel H, Heinen HJ (1980) Carbon in solid solution in forsterite-A key to the untractable nature of reduced carbon in terrestrial and cosomogenic rocks. Geochim Cosmoch Acta 44:1319–1333

Freund F, Wengeler H, Kathrein H, Knobel R, Oberheuser G, Maiti G, Reil D, Knipping U, Kotz J (1983) Hydrogen and Carbon derived from dissolved H_2O and CO_2 in minerals and melts. Bull Mineral 106:185–200

Frey FA, Prinz M (1978) Ultramafic inclusions from San Carlos, Arizona: Petrologic and Geochemical data bearing on their petrogenesis. Earth Planet Sci Lett 38:129–176

Frey FA, Green DH (1974) The mineralogy geochemistry and origin of lherzolite inclusions in Victorian basanites. Geochim Cosmochim Acta 38:1023–1059

Fujii T, Scarfe CM (1982) Petrology of Ultramafic Nodules from West Kettle River, near Kelowna, Southern British Colombia. Contrib Mineral Petrol 80:297–306
Ghent ED, Coleman RG, Hadley DG (1980) Ultramafic inclusions and host Alkali Olivine basalts of the Southern Coastal Plain of the Red Sea, Saudi Arabia. Am J Sci 280-A:499–527
Grove TL (1982) Use of exsolution lamellae in lunar clinopyroxene as cooling rate speedometers: an experimental calibration. Am Mineral 67:251–268
Hamilton DL, Burnham CW, Osborn EF (1964) The solubility of water and effects of oxygen of water and effects of oxygen fugacity and water content on crystallization in mafic magmas. J Petrol 5:21–39
Harte B (1983) Mantle peridotites and processes – the kimberlite sample. In: Hawkesworth CJ, Norry MJ (eds). Continental Basalts and Mantle Xenoliths. Shiva Publ Co. 46–91
Hauksson E (1983) Episodic Rifting and Volcanism at Krafla in North Iceland: Growth of Large Ground Fissures along the plate Boundary. J Geophys Res 88:625–636
Helgeson HC, Kirkham (1974) Theoretical Prediction of the Thermodynamic behavior of aqueous electrolytes at high Pressures and Temperatures: I: Summary of the Thermodynamic/electrostatic properties of the Solvent. Am J Sci 274:1089–1198
Hill DP (1977) A Model for Earthquake Swarms. J Geophys Res 82:1347–1352
Hodges FN (1974) The solubility of H_2O in silicate melts. Carnegie Inst Wash Yearb 73:251–255
Hofmann AW, Magaritz M (1977) Diffusion of Ca, Sr, Ba, and CO in a basalt melt: Implications for the Geochemistry of the mantle. J Geophys Res 82:5432–5438
Holloway JR (1977) Fugacity and activity of molecular species in supercritical fluid. In: Fraser D, Reidel D (eds). Thermodynamics in Geology. Dordrecht-Holland, pp 161–181
Horton RM, Horton MD (1972) The high-pressure graphitization of diamond. High Temperatures – High Pressures 4:39–48
Housley RM (1978) Modelling Lunar Eruptions. Proc 9th Lunar Planet Sci Conf 1473–1484
Irving AJ (1980) Petrology and Geochemistry of composite ultramafic xenoliths in alkalic basalts and implications for magmatic processes within the mantle. Am J Sci 208-A:389–426
Kadik AA, Lukanin OA, Lebedev YB, Korovushkina E (1972) Solubility of H_2O and CO_2 in granite and basalt melts at high pressures. Gokhimiya 12:1549–1560 (in Russian)
Kadik AA, Lebeder YB (1969) Temperature dependence of the solubility of water in an albite melt at high pressures, Geochim Int 73:6023–6029
Kay JM (ed) (1968) An Introduction to Fluid Mechanics and Heat Transfer 2nd. Cambridge University Press
Kerrick DM, Jacobs GK (1981) A modified Redlich-Kwong Equation for H_2O, CO_2 and H_2O-CO_2 mixtures at elevated pressures and temperatures. AJS 281:735–767
Khitarov NI, Lebedev EB, Regartan EV, Arseneva RV (1959) Solubility of water in basaltic and granitic melts. Geochemistry 5:479–492
Kleeman JD, Green DH, Lovering JF (1969) Uranium distribution in ultramafic inclusions from Victorian basalts. Earth Planet Sci Lett 5:449–458
Klein FW (1982) Earthquakes at Loihi Submarine Volcano and the Hawaiian Hot Spot. J Geophys Res 87:7719–7726
Klein FW, Einarsson P, Wyss M (1977) The Reykjanes Peninsula, Iceland, Earthquake swarm of September 1972 and its tectonic significance. J Geophys Res 82:865–888
Lang AR (1972) Pressure and temperature gradients in ascending fluids and magmas. Nature 238:98–100
Littlejohn AL, Greenwood HJ (1974) Lherzolite nodules in basalts from British Columbia, Canada. Can J Earth Sci 11:1288–1308
Lovelace RW (1984) Origins of fluid and glass inclusions in mafic and ultramafic xenoliths from volcano Teneguia, La Palma, Canary Islands, Spain. Unpubl A.B. Thesis, Princeton University, pp 76
Marsh BD (1981) On the Crystallinity, Probability of Occurrence, and rheology of Lava and Magma. Contrib Mineral Petrol 78:85–98
Marsh BD (1978) On the cooling of ascending andesitic magma. Phil Trans R Soc Lond A 288:611–625
Marsh BD, Kantha LH (1978) On the Heat and Mass Transfer from an Ascending Magma. Earth Planet Sci Lett 39:435–443
Marsh BD (1976) Mechanics of Benioff Zone magmatism. In: Sutton GH, Manghani MH, Moberly RH (eds). Geophysics of the Pacific Ocean and its Margin. Am Geophys Union 19:337–350
McCallister RH, Meyer HOA, Aragon R (1979) Partial thermal history of two exsolved clinopyroxenes from the thaba Putsoa kimberlite pipe, Lesotho. In: Boyd FR, Meyer HO (eds). The mantle Sample: Inclusions in kimberlites and other volcanics, vol 2. Am Geophys Union, Washington, D.C., USA
McGetchin TR, Ullrich GW (1973) Xenoliths in Maars and Diatremes with inferences for the Moon, Mars and Venus. J Geophys Res 78:1833–1854
McGetchin TR, Nikhanj YS (1973) Carbonatite-Kimberlite Relations in the Cane Valley Diatreme, San Juan County, Utah. J Geophys Res 78:1854–1868
Mercier JC (1979) Peridotite xenoliths and the dynamics of kimberlites intrusion. In: Boyd FR, Meyer HO (eds). The Mantle Sample: Inclusions in Kimberlites and other Volcanics, vol 2. Am Geophy Union Washington, D.C., USA
Millhollen GL, Irving AJ, Wyllie PJ (1974) Melting Interval of peridotite with 5.7 percent water to 30 kilobars. J Geol 82:575–587
Millhollen GL, Wyllie PJ (1974) Melting Relations of brown hornblende mylonite from St. Paul's Rocks under water saturated and water undersaturated conditions to 30 kilobars. J Geol 82:589–606
Morris S (1982) The effects of a strongly temperature-dependent viscosity on slow flow past a hot sphere. J Fluid Mech:1–26
Murase T, McBirney AR (1973) Properties of some common igneous rocks and their melts at high temperatures. Geol Soc Am Bull 84:3563–3592
Murck B, Burruss R, Hollister L (1978) Phase equilibrium in fluid inclusions in ultramafic xenoliths. Am Mineral 63:40–46
Nelson SA, Carmichael ISE (1979) Partial Molar Volumes of oxide components in Silicate Liquids. Contrib Mineral Petrol 71:117–124
Nicholls J (1980) A Simple Thermodynamic Model for estimating the solubility of H_2O in magmas. Contrib Mineral Petrol 74:211–220
Oberheuser G, Kathrein H, Demortier G, Gonska H, Freund F (1983) Carbon in olivine single crystals analyzed by the $^{12}C(d,p)^{13}C$ method and by photoelectron spectroscopy. Geochim Cosmochim Acta 47:1117–1129
O'Hara MJ, Richardson SW, Wilson G (1971) Garnet peridotite stability and occurrence in crust and mantle. Contrib Mineral Petrol 32:48–68
Oxtoby S, Hamilton DL (1978) Calculation of the solubility of water in granitic melts. In: Mackenzie WS (ed) Progress in Experimental Petrology, Natural Environment Research Council, Great Britain, 4th Progress Report. pp 37–40
Pinkerton H, Sparks RS (1978) Field Measurements of the Rheology of lava. Nature 276:383–385
Roedder E (1965) Liquid CO_2 inclusions in olivine-bearing nodules and phenocrysts from basalts. Am Mineral 50:1746–1782
Rohsenow WM, Choi HY (1962) Heat Mass and Momentum Transfer. Prentice-Hall, New Jersey, p 537
Ryabchikov ID, Schreyer W, Abraham K (1982) Compositions of Aqueous Fluids in Equilibrium with Pyroxene and Olivines at Mantle Pressures and Temperature. Contrib Mineral Petrol 79:80–84
Ryabchikov ID, Boettcher AL (1980) Experimental Evidence at high Pressure for potassic metasomatism in the mantle of the Earth. Am Mineral 65:915–919
Ryan MP, Blevins JYK, Okamura AT, Koyanagi RY (1983) Magma reservoir subsidence mechanics theoretical summary

and application to Kilauea Volcano, Hawaii. J Geophys Res 88:4147–4181
Scarfe CM (1973) Water Solubility in basic and ultrabasic magmas. Nature Phys Sci 246:9–10
Shames IH (1982) Mechanics of Fluids. 2nd Ed, McGraw Hill, New York, p 725
Shapiro AH (1953) The Dynamics and Thermodynamics of Compressible Fluid Flow. Vol 1, John Wiley, New York, p 647
Sharp WE (1962) The Thermodynamic functions for water in the range – 10 to 1,000° C and 1 to 250,000 bars, Livermore, Calif. Univ Calif Lawrence Rad Lab, UCRL-7118, p 51
Shaw HR (1980) The fracture mechanisms of magma transport from the mantle to the surface. In: Hargraves RB (ed). Physics of Magmatic Processes. Princeton University Press, Princeton. pp 201–264
Shaw HR (1974) Diffusion of H_2O in granitic liquids, Part I, Experimental data; Part II, Mass transfer in magma chambers. In: Hoffman AW, Gilletti BJ, Yoder HS, Yund RA (eds). Geochemical Transport and Kinetics. Carnegie Inst Wash Yearb:139–170
Shaw HR (1972) Viscosities of magmatic silicate liquids: an empirical method of prediction. Am J Sci 272:870–893
Shaw HR (1969) Rheology of basalt in the melting range. J Petrol 10:510–535
Shaw HR, Peck DL, Wright TL, Okamura R (1968) The viscosity of basaltic magma: An analysis of field measurements in Makaopuhi lava lake. Hawaii. Am Jour Sci 266:255–264
Shaw HR (1965) Comments on viscosity, crystal settling and convection in granitic systems. Am J Sci 272:120–152
Shmonov VM, Shmulovich KI (1974) Molal volumes and CO_2 at temperatures from 100–1,000° C and pressures. Doklady Akad Nauk SSSR 217:206–209
Shmulovich KI, Shmonov VM (1975) Fugacity coefficients for CO_2 from 1.0132 to 10,000 bar and 450–1,300° K. Geokhimiya 4:551–555
Sibree JO (1934) The viscosity of froth. Faraday Soc Trans 30:325–331
Smyth JR, Hatton CJ (1977) A Coesite-Sanidine Grospydite from the Roberts Victor Kimberlite. Earth Planet Sci Lett 34:284–290
Solovova IP, Ryabchikov ID, Kovalenko VI, Naumov VB (1982) High density CO_2 inclusions in mantle lherzolite. Doklady Akademii Nauk SSSR 263:179–182
Sparks RS, Pinkerton H, MacDonald R (1977) The transport of xenoliths in magmas. Earth Planet Sci Lett 35:234–238
Spence DA, Turcotte DL (1983) A magma fracture model for magma migration and the injection of dikes and sills, EOS. Trans Am Geophys Union 64:850
Spence DA, Turcotte DL (1984b) Magma driven propagation of cracks. Preprint
Spengler CJ, Burnham CW (1966) Cuoted by Clark (1966): Solubility In: Clark SP Jr (ed) Handbook of Physical Constants. Geol Soc Am Mem 97:415–436
Spera FJ, Yuen DA, Kirschvink SJ (1982) Thermal boundary layer convection in Silicic Magma Chambers: Effects of Temperature dependent Rheology and Implications for Thermogravitation Chemical fractionation. J Geophys Res 87:8755–8667
Spera FJ (1982) Ascent and Eruption of Alkali Basalt: Energetics and Dynamics. Geol Soc Am Abstr Prog 15:7
Spera FJ (1981) Carbon Dioxide in Igneous Petrogenesis II: Fluid dynamics of mantle metasomatic processes. Contrib Mineral Petrol 77:56–65
Spera FJ (1980) Aspects of Magma Transport. In: Hargraves R (ed) Physics of Magmatic Processes. Princeton University Press, Princeton, NJ, pp 265–323
Spera FJ, Bergman SC (1980) Carbon Dioxide in Igneous Petrogenesis: I. Contrib Mineral Petrol 74:55–66
Spera FJ (1977) Aspects of the Thermodynamic and Transport Behavior of Basic Magmas, Ph.D. Dissertation Unpublished, University of California at Berkeley
Spera FJ (1974) A thermodynamic basis for predicting water solubilities in silicate melts and implications for the low velocity zone. Contrib Mineral Petrol 45:175–186
Stern CR, Wyllie PJ (1973) Water-saturated and undersaturated melting relations of a granite to 35 kilobars. Earth Planet Sci Lett 18:163–7
Stevenson DJ (1983) Magmatic transport by the migration of fluid-filled cracks. EOS Trans Am Geophys Union (abstr) 64:848
Stolper E (1982) On the speciation of water in silicate melts. Geochim Cosmochim Acta 46:2609–2620
Stolper E, Walker D, Hager BH, Hays JF (1981) Melt Segregation from partially molten source regions: The importance of melt density and source region size. J Geophys Res 86:6261–6271
Swanson DA, Wright TL, Helz RT (1975) Linear vent systems and estimated rates of magma production and eruption for the Yakima basalt on the Columbia Plateau. Am J Sci 275:877–905
Vilminot JC (1965) Les enclaves dee peridotite et de pyroxenite a spinelle dans le basalte du Rocher du Lion (Chaine du Deves – Haute Loire. Soc Franc Mineral Cristallogr Bull 88:109–118
Walker GPL (1958) Geology of the Reydarfjordur area, eastern Iceland: Geol Soc Lond Quart J 114:367–390
Wallis GB (1969) One-dimensional Two-phase Flow. McGraw-Hill, New York, p 408
Wanamaker BJ, Bergman SC, Evans B (1982) Crack Healing in Silicates: Observations on Natural lherzolite Nodules. Trans Am Geophys Union 63:437
White RW (1966) Ultramafic inclusions in basaltic rocks from Hawaii. Contrib Mineral Petrol 12:245–314
Wilson L, Sparks RSJ, Walker GPL (1980) Explosive volcanic eruptions-IV. The control of magma properties and conduit geometry on eruption column behavior. Geophys J R Astron Soc:117–148
Wyllie PJ (1980) The origin of kimberlite. J Geophys Res 85:6902–6910
Wyllie PJ (1979) Magmas and volatile components. Am Mineral 64:469–500
Wyllie PJ (1978) Mantle fluid Compositions buffered in peridotite CO_2-H_2O by carbonates, amphibole, and phlogopite. J Geol 86:687–713
Wyllie PJ, Huang WL (1976) High CO_2 solubilities in mantle magmas. Geology 4:21–24

Received March 27, 1984; Accepted June 16, 1984